buildings

MDPI

Article

Fire Load Effects on Concrete Bridges with External Post-Tensioning: Modeling and Analysis

Michele Fabio Granata [1,*], Zeno-Cosmin Grigoraş [2] and Piero Colajanni [1]

[1] Dipartimento di Ingegneria, Università di Palermo, 90128 Palermo, Italy; piero.colajanni@unipa.it
[2] Faculty of Civil Engineering and Building Services, "Gheorghe Asachi" Technical University of Iasi, 700050 Iași, Romania; zeno-cosmin.grigoras@academic.tuiasi.ro
* Correspondence: michelefabio.granata@unipa.it

Abstract

The fire performance of existing reinforced concrete (RC) bridge decks strengthened by external prestressing systems is investigated, with particular attention to the vulnerability of externally applied tendons under realistic fire scenarios. Fire exposure represents a critical condition for such retrofitted structures, as the structural response is strongly influenced by load level, prestressing effectiveness, and thermal degradation of the strengthening system. A comprehensive assessment framework is proposed, combining thermal and mechanical analyses applied to representative highway overpass bridges. The thermal input adopted for the analyses is first validated through computational fluid dynamics (CFD) simulations, aimed at evaluating temperature development in typical RC beam–girder grillage decks subjected to fire from below. The CFD study considers variations in clearance height and span length and confirms that, in the case of hydrocarbon tanker accidents with fuel spilled on the roadway, conventional fire curves commonly adopted in the literature provide a reliable and conservative representation of both the temperature levels reached and their rate of increase within structural elements, thus supporting their use for rapid and simplified assessments. The validated thermal input is then employed in an analytical fire safety procedure applied to several realistic bridge case-studies. A parametric investigation is carried out by varying deck geometry, span length, reinforcement layout, and the presence of external prestressing retrofit, allowing the evaluation of the reduction in bending capacity and the time-dependent degradation of mechanical properties under fire exposure. The results highlight the critical role of external prestressing in fire scenarios, showing that significant loss of prestressing effectiveness may occur within the first minutes of fire, potentially leading to critical conditions even at service load levels. Finally, a multi-hazard assessment is performed by combining fire effects with pre-existing aging-related deterioration, such as reinforcement corrosion and long-term prestressing losses, demonstrating a marked increase in failure risk and, in the most severe cases, the possibility of premature collapse under dead loads.

Keywords: structural assessment; CFD analysis; fire; bridges; prestressing

Check for updates

Academic Editor: Marina Gravit

Received: 5 January 2026
Revised: 17 January 2026
Accepted: 19 January 2026
Published: 20 January 2026

Copyright: © 2026 by the authors. Licensee MDPI, Basel, Switzerland. This article is an open access article distributed under the terms and conditions of the Creative Commons Attribution (CC BY) license.

1. Introduction

Fire-induced failures of bridges are increasingly reported and, in several contexts, appear more frequent than those caused by other extreme actions such as earthquakes, wind, floods, or snow [1]. Despite this evidence, fire remains marginally addressed in bridge design and is often excluded from Ultimate Limit State (ULS) checks, particularly

for RC bridges. Severe fires, often associated with vehicle or tanker accidents, have shown that this assumption can be unconservative, especially for road overpasses exposed to fire from below.

Statistical analyses of bridge collapses in the United States consistently indicate that fire-related events account for a small but non-negligible fraction of cases. Large-scale studies report that approximately 2.8–3.2% of bridge collapses are attributable to fire, with some surveys reporting values as high as 4.9%. Although significantly less frequent than hydraulic or impact-related causes, fire-induced collapses are comparable to, and in some cases exceed, those associated with seismic actions [2–4].

While documented fire incidents indicate that major structural damage predominantly affects steel and composite bridges [3–5], RC bridges are generally considered less vulnerable due to the inherent fire resistance of concrete. However, this may not hold when prestressing systems are involved. In prestressed concrete bridges, prolonged fire exposure and high thermal loads can rapidly degrade prestressing steel, resulting in sudden prestressing loss and severe reductions in structural capacity, potentially reaching the Service Limit State (SLS) for excessive deformations, Ultimate Limit State (ULS), or even collapse [6–8]. Accidents involving hydrocarbon tankers near or beneath bridges and viaducts have caused severe structural damage, in some cases leading to partial or total collapse. Representative examples include the collapse of the I-85 bridge in Atlanta [3] and the fire-induced damage to the Caogou Bridge in China [5], both built with prestressed concrete girders.

In these events, the structural response to fire—typically associated with hydrocarbon fires characterized by quick temperature rise and sustained exposure in the range of 800–1000 °C—depends primarily on the structural system and the bridge components directly affected, highlighting the importance of targeted fire risk assessments.

An illustrative case is the collapse of the McArthur Maze Bridge [2], for which CFD simulations were performed to estimate the potential temperatures reached during the fire event. Literature studies have shown that, despite minor fluctuations, the temperature profile obtained from fluid mechanics–based thermal analysis for that case closely aligns with the Eurocode model for hydrocarbon fires, thus supporting the applicability of such analyses in similar scenarios, which can be considered representative of worst-case conditions for temperature rise in safety assessments.

This issue, generally less important for concrete bridges, becomes particularly critical for RC bridges strengthened by external prestressing, increasingly adopted in both new construction and retrofit, and consisting of external unbonded tendons [9–11] placed outside the concrete section, typically protected only by polymeric sheaths with or without grease infill. These tendons govern structural response from service to failure while representing the most fire-exposed component [12]. Fire-induced degradation may trigger a sudden transition from the prestressed to the original RC structure, followed by progressive capacity loss.

Increasing attention has been directed toward multi-hazard scenarios that combine fire with other risks, such as concrete aging and reinforcement corrosion. The timing of prestress loss during a fire event and the remaining safety margins are critical for fire safety and emergency management, as quick initial degradation can exacerbate the effects of pre-existing deterioration.

Most studies have focused on steel or composite structures [13], individual prestressing strands [14,15], or internally prestressed RC bridges [16–18]. Only a few have addressed externally prestressed RC bridges that lose their strengthening capacity due to fire [19–22], where the timing of the transition from prestressed to unprestressed conditions and the associated safety factors are of fundamental importance.

In this study, fire inputs are derived and validated through CFD simulations, capturing realistic fire scenarios for typical RC overpasses. The thermal fields obtained from CFD are used to define equivalent fire loads for thermo-structural analyses aimed at evaluating prestressing degradation and bearing capacity loss. Results from previous experimental campaigns on scaled beams [23] support the numerical modeling of structural behavior. The approach is applied to realistic bridge case studies, incorporating parametric variations in deck geometry, reinforcement, and external prestressing, thereby enabling the assessment of fire-induced performance degradation up to ULS and collapse. This simplified methodology is particularly valuable for the risk assessment of large inventories of highway overpasses with repetitive geometries.

The novelty of the study lies in combining CFD-validated fire inputs with structural analyses under fire exposure, explicitly addressing externally prestressed RC bridges and facilitating a multi-risk perspective that integrates pre-existing deterioration, fire-induced prestress loss, and residual structural capacity.

2. Fire Load Beneath Overpasses

This section aims to numerically simulate fire development on a specific type of road bridge using Computational Fluid Dynamics (CFD), and to benchmark the results against fire loads reported in the literature and design codes. The analysis considers variations in fire location and intensity, applying an advanced numerical framework to model fire effects and determine the resulting temperature distribution across the concrete deck.

2.1. Geometry of the Bridges and Input Data

The geometry of the two case-study bridges is illustrated in Figure 1. Both are RC overpasses composed of five beams (with spans of 10 m and 15 m between bearing supports) strengthened by external post-tensioned tendons. Each beam is retrofitted with two tendons, each consisting of four strands with a 15 mm diameter. The traffic clearance is 6.00 m for the bridge with 10 m spans and 8.00 m for the bridge with 15 m spans. The underlying carriageways measure 7.5 m and 10.5 m in width, respectively. Figure 1a,b present elevation views of the 10 m-span bridge, while Figure 1c,d depict the 15 m-span bridge. The upper deck is supported by wall piers or multi-column bent piers, resulting in a highly confined environment beneath the overpasses, compared to bridges placed in an open environment.

The fire scenarios considered involve an accident in which a fuel tanker passes beneath the RC structure. In the event of damage, fuel is spilled onto the road surface. Gasoline is assumed as the fuel for this analysis, and three different spill scenarios on the road surface are examined:

- FS1: the fuel spilled only beneath the RC overpass.
- FS2: the fuel spilled beneath the RC overpass and extended to 3.75 m on both sides.
- FS3: the fuel spilled beneath the RC overpass and extended to 7.50 m on both sides.

The value of 3.75 m represents half of the structure's transverse width, while 7.50 m represents the total transverse width of the overpass deck.

Gasoline was selected as the representative fuel for this study due to its prevalence in road transport and its high volatility. From a fire safety engineering perspective, gasoline represents a "worst-case" liquid fuel spill because of its low flash point—facilitating rapid ignition compared to diesel—and its high specific heat of combustion. By adopting this fuel type, the simulations establish a conservative thermal envelope, ensuring that the structural assessment accounts for the most severe heat release rates typically encountered in highway fuel-tanker accidents.

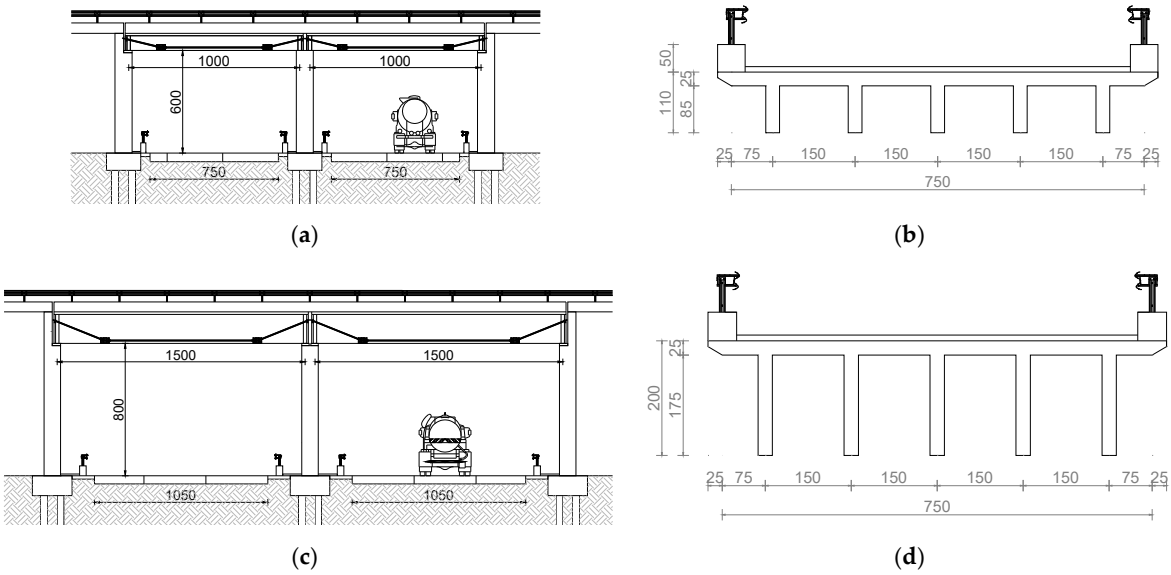

Figure 1. Geometry of the overpass bridges taken as case studies (measures in cm). (**a**) Lateral view and underneath the road for the bridge with a 10 m span. (**b**) Geometry of the RC deck cross-section for the bridge with 10 m span. (**c**) Lateral view and underneath the road for the bridge with a 15 m span. (**d**) Geometry of the RC deck cross-section for the bridge with a 15 m span.

2.2. Fire Loads Derived from CFD Models

The fire model employed is a Natural Fire—Advanced Fire—CFD model, in accordance with the European classification of fire models [24]. In recent years, numerical simulations of fires using the Performance-Based Approach (PBA) and CFD models have become increasingly common for evaluating fire behavior and its impact on structures, allowing for more accurate predictions of temperature evolution, fire spread, and structural response [25,26].

The research employs FDS v6.8.0 (Fire Dynamics Simulator) software, which numerically solves a form of the Navier–Stokes equations suitable for low-speed, thermally driven flows, with particular emphasis on smoke and heat transport from fires [27–30].

The modeled fuel is gasoline with the following parameters:

- Net heat of combustion is 43.70 (MJ/kg) [31].
- Mass burning rate per unit area is 0.055 (kg/m^2 s) [32].
- Considered "ramp-up time" set to default 1 s. It has been considered that the entire burning surface is quickly ignited and the fire reaches its peak Heat Release Rate in a short period of time. The study focuses only on the average temperature of the fire, not on when the maximum temperature is reached.
- Energy is ideal and did not take into account CO, H_2, or Soot. Due to different types of gasoline (leaded, unleaded, different additives, different proportions of ethanol, etc.), the CO, H_2, and Soot yield may vary significantly [27]. This approach will generate slightly more effective heat of combustion that can be seen as a safety margin for this study.

The combustion process is characterized by prescribing the fundamental material properties of gasoline—net heat of combustion and mass loss rate—rather than imposing a fixed Heat Release Rate (HRR) curve from the literature. This approach allows FDS to dynamically compute the Heat Release Rate (HRR) based on local environmental conditions. Consequently, the simulation accounts for combustion inefficiencies and oxygen limitations inherent to the bridge's geometry and ventilation, ensuring that the energy output remains physically consistent with a real-world liquid spill scenario.

A mesh sensitivity study was performed to analyze the best cell size suited for these cases [27,30]. The authors had run different tests with 1.50 (m), 0.375 (m), and 0.25 (m) cubic cell size but in the end, the decision of using 0.75 × 0.75 × 0.75 (m) was made because it better approximates the real geometry, the simulation time was reasonable, and numerical instability was avoided. For each fire scenario considered, all the input parameters are kept the same; only the burning surface is modified, as shown in Table 1. The burning surface is centered under the RC overpass; the simulation time is 3600 s.

Table 1. Dimensions of burning areas in different fire scenarios.

Fire Load Scenario	Dimensions [m]	Burning Area [m^2]
FS1	10.50 × 7.50	78.50
FS2	10.50 × 15.00	157.50
FS3	10.50 × 22.50	236.25

To accurately simulate the atmospheric condition of an unconfined bridge fire, all external boundaries of the computation domain (excluding the road surface) were defined as "open". This configuration ensures that fire development is strictly fuel-controlled by allowing a pressure-driven exchange of air and combustion products with the ambient environment [27,28]. By adopting these boundary conditions, the model replicates a realistic scenario where smoke and heat are free to dissipate, preventing the artificial heat accumulation that would occur in a confined or semi-confined space.

Regarding the structural surfaces, such as the beams and the deck slab, they were characterized using "inert" boundary conditions. This assumption, while maintaining the surface temperature at the initial ambient value of 20 (°C) [27], is justified by the high thermal inertia of the massive concrete sections, which prevents the surface temperature from significantly influencing the gas-phase fire dynamics during the short-term fire exposure. The CFD simulations are primarily intended to capture the incident heat flux as conservative input for the subsequent thermal-mechanical model, where the concrete internal heat conduction is fully accounted for.

The fire source, representing a gasoline spill on the asphalt, is modeled using a "vent" with a "burner" surface attribute [27,28]. This method simulates the fire by injecting a stoichiometric fuel vapor into the computational domain at a rate calibrated to match the target Heat Release Rate (HRR) of the scenario. This injected gas then reacts with atmospheric oxygen, allowing for realistic development of the fire plume and the subsequent convective and radiative heat transfer to the bridge structure. This approach effectively captures the thermal power of the fire without the need to model the complex phase-change physics of the liquid fuel.

As a result, the temperature was monitored in the middle of the RC overpass in two different positions: 1 cm under the web of the RC beam and 1 cm under the flange of the RC beam. The computation domain for each fire scenario is shown in Figure 2.

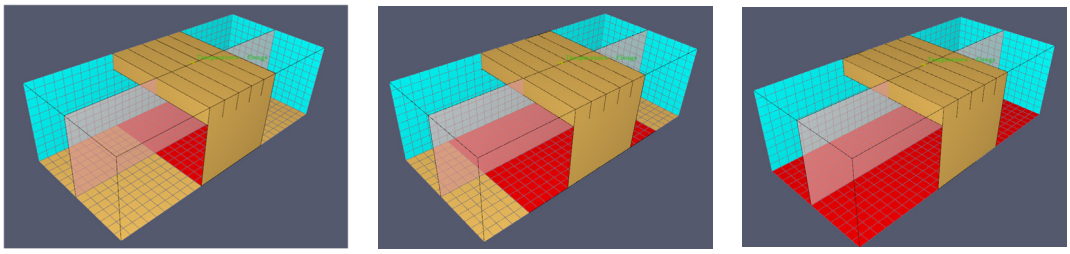

(**a**) (**b**) (**c**)

Figure 2. Fire scenarios for different burning areas. Red area is the burning one. (**a**) FS1, (**b**) FS2, (**c**) FS3.

The analyzed parameter is temperature (°C) measured in the center of the RC overpass, and it is presented as a 2D slice in Figure 3. For each fire scenario, the maximum temperature is under the RC overpass. For fire scenarios, FS2 and FS3, very high temperatures are registered near the analyzed structure. Due to the "open-mesh boundaries" setup (air intake and hot gas exhaust), low temperatures are registered near the boundaries of the computational domain, except for the road surface where the fuel is burning.

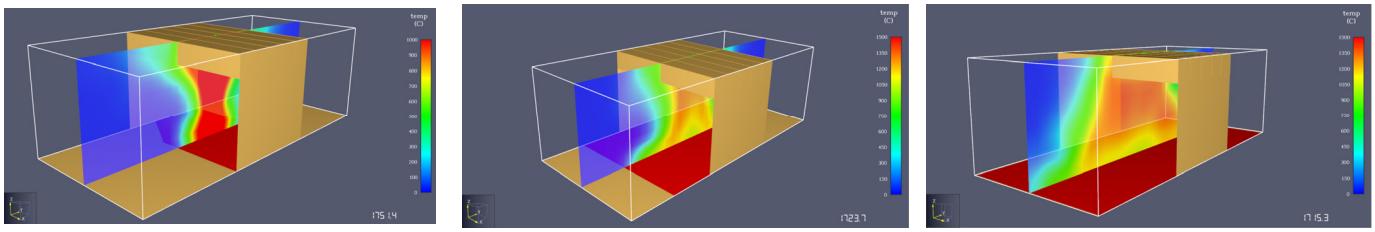

(**a**) (**b**) (**c**)

Figure 3. Results of temperatures, CFD analysis. (**a**) Scenario FS1, (**b**) Scenario FS2, (**c**) Scenario FS3.

For each fire Scenario, the temperature measured under the RC beam flange is significantly higher (about 300 °C) compared with the temperature measured at the RC beam web (Figure 4); this is due to the geometry of the grillage deck. For each case, temperature variation of about +/−50 °C is due to the air intake and gas exhaust in/from the computational domain (which best simulates the real air-hot gases flow). Maximum values of temperature are registered under the flange in the fire scenario FS3.

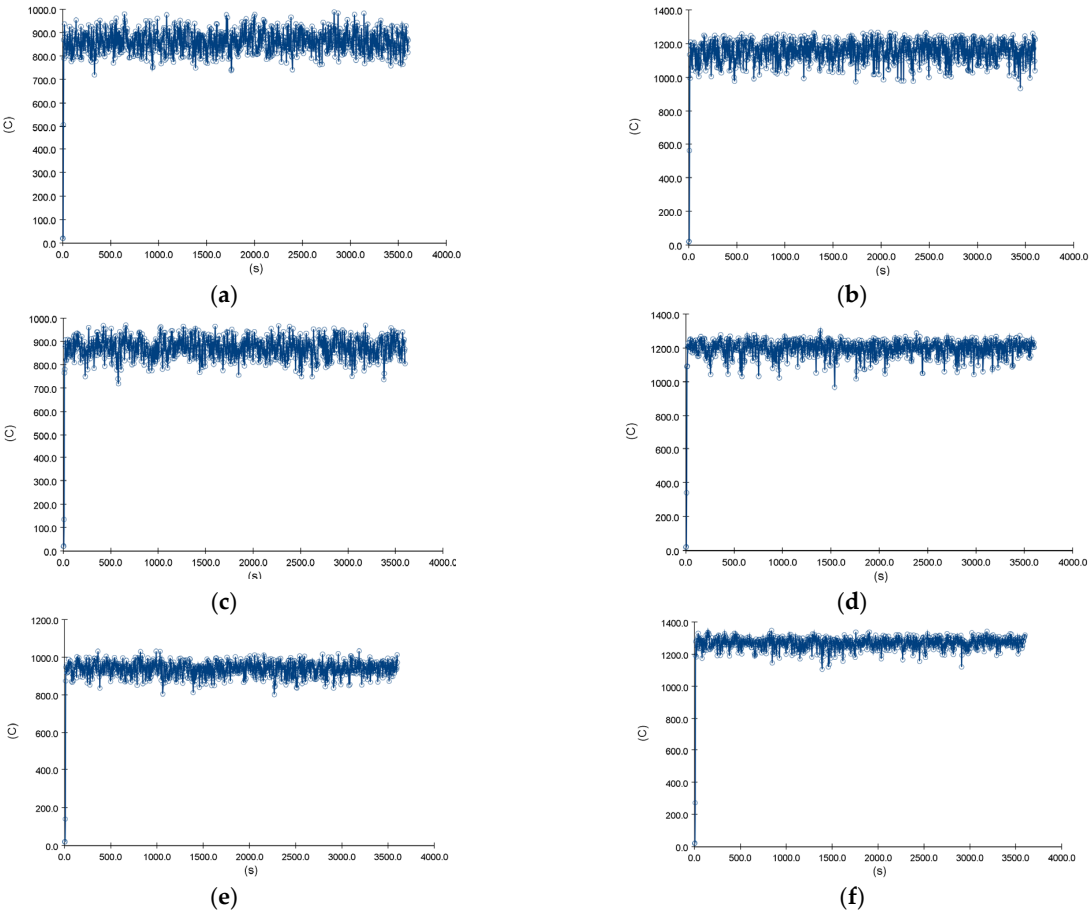

Figure 4. Temperature-time diagrams on the web and the bottom flange of the girder for the different scenarios. (**a**) FS1, web; (**b**) FS1, flange; (**c**) FS2, web; (**d**) FS2, flange; (**e**) FS3, web; (**f**) FS3, flange.

2.3. Comparison Between Numerical Fire Curves and Literature Data

All previously computed temperatures are compared (Figure 5) with those derived from the conventional fire models of Eurocode 1 [24], including the standard fire, exterior fire, and hydrocarbon fire curves. The temperature profiles obtained from the CFD simulations are superimposed on the conventional curves in Figure 6 for beam flanges and webs. Considering the input "ramp-up function" of 1 s, the CFD fire model used represents a single-stage fire, modeling the fully developed stage. The conventional fire models consist of the following stages:

- Standard fire, single-stage model: only the growth stage is considered. The maximum temperature reaches 945 °C at 3600 s. This model is intended for enclosed or highly confined spaces, such as buildings.
- Exterior fire, two-stage model: both growth and fully developed stages are considered. The maximum temperature is 680 °C. This model is typically used for exterior structural elements where the fuel is not hydrocarbon-based.
- Hydrocarbon fire, two-stage model: both growth and fully developed stages are considered. The maximum temperature is 1100 °C. This model is intended for exterior structural elements exposed to hydrocarbon fuels.

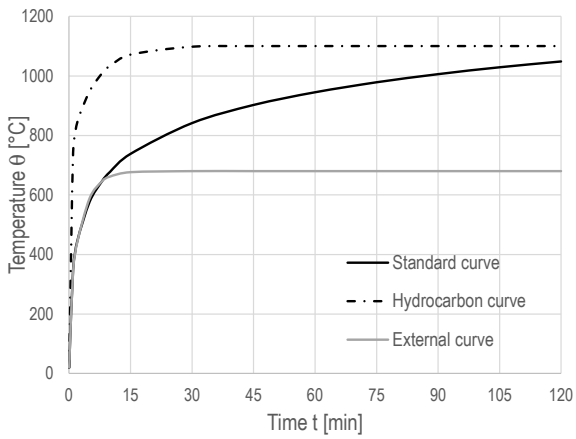

Figure 5. Eurocode conventional fire curves.

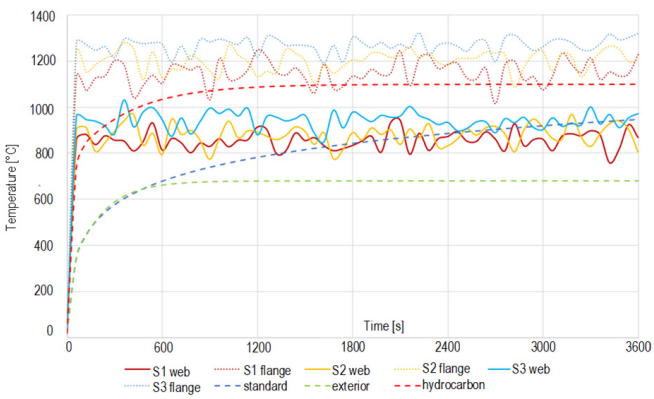

Figure 6. Temperature-time diagrams and comparison with literature curves for the first hour of burning.

The average computed temperatures and heat release rates (HRR) are reported in Table 2. Scenario FS1 yields the lowest temperature and the highest HRR, while Scenario FS3 exhibits the highest temperature and the lowest HRR.

Table 2. Average computed temperature and average computed HRR.

Fire Scenario	Web [°C]	Flange [°C]	HRR [kW/m^2]
FS1	860	1151	2024
FS2	870	1194	1833
FS3	936	1265	1782

Results from the CFD analysis indicate that, in the event of a hydrocarbon tanker fire beneath a highway overpass, the deck elements (beam flanges and webs) are exposed to high temperatures. These temperatures increase rapidly during the early stages of ignition and remain elevated for the duration of fuel combustion, which in the simulations extends up to one hour.

The peak temperatures predicted by the CFD simulations are comparable to those derived from literature fire curves, particularly the hydrocarbon curve for the most severe scenarios and the standard curve for less severe cases. However, the initial temperature rise in the standard curve is considerably slower, resulting in a less realistic representation of such accidents. Nevertheless, the literature-based curves remain suitable for simplified and rapid analyses, as they do not introduce significant deviations from the temperature evolution observed in the deck's structural elements via CFD. For given temperature levels, these curves provide an adequate approximation of structural response and fire-induced degradation, which can subsequently be correlated with the evolution of mechanical behavior under fire.

3. Structural Model and Analyses of RC Bridges Strengthened by External Prestressing

3.1. Analysis of Case-Study Bridges

The two deck types illustrated in Figure 1, with span lengths of 10 m and 15 m, were investigated as representative of overpass configurations with clearance heights of 6 m and 8 m. This parametric approach allows a comparative assessment of structural behavior with respect to span variation, the proportion of reinforcement affected by fire-induced damage relative to the structural concrete cross-section, and the influence of external prestressing on the two decks. The comparison is conducted under equivalent total prestressing axial forces, allowing for a separate evaluation of thermal, geometric, and mechanical effects. The structural performance was evaluated by considering the progressive reduction in capacity induced by temperature effects, with a focus on the time evolution of the ultimate bending moment, $M_{u,L}$, of the midspan cross-section. The initial reduction affects the strengthened beam equipped with a sheathed external tendon, due to both thermal degradation and prestressing relaxation. Once the strengthening system is deemed ineffective, the analysis refers to the original RC section without prestressing, accounting for the temperature-dependent strength reduction in the bottom mild steel reinforcement.

The first stage of the assessment concerns the loss of prestressing caused by heating of the steel tendon. This evaluation explicitly considers the tendon cross-sectional area as well as the thickness and material properties of the protective sheath. The heating delay of the protected steel element was determined in accordance with Equation 4.27 of Eurocode 3 [33], incorporating the thermal properties of the plastic sheath. This equation allows the temperature of a steel cross-section insulated by fire-protective material to be evaluated, and it is reported below:

$$\theta_{a,t} = \frac{\lambda_p \, A_p/V}{d_p \, c_a \, \rho_p} \frac{\left(\theta_{g,t} - \theta_{a,t}\right)}{1 + \phi/3} \Delta t - \left(e^{\phi/10} - 1\right) \Delta\theta_{g,t} \quad (1)$$

where

$\phi = \frac{c_p\,\rho_p}{c_a\,\rho_a} d_p\ A_p/V$;
A_p fire-protective material of tendon per unit length of the element $\left[\mathrm{m}^2/\mathrm{m}\right]$;
V volume of the element per unit length $\left[\mathrm{m}^3/\mathrm{m}\right]$;
A_p/V section factor $\left[\mathrm{m}^{-1}\right]$;
d_p thickness of the fire-protective material [m];
$\theta_{a,t}$ steel temperature at time t [°C];
$\theta_{g,t}$ gas temperature in the surrounding environment at time t [°C];
$\Delta\theta_{g,t}$ increase in the temperature of the gases during the time interval Δt [°C];
Δt considered time interval [s], assumed equal to 30 s;
ρ_a density of steel $\left[\mathrm{kg}/\mathrm{m}^3\right]$, taken as 7850 kg/m^3;
c_a specific heat capacity of steel, varying as a function of the temperature reached during the fire, according to Chapter 3 of Eurocode 3 [J/(kg K)].

The protective material considered for the prestressing tendon is a plastic tube made of high-density polyethylene (HDPE) with a thickness of 5 or 15 mm. The thermal properties of the protective material are the following:

ρ_p density of the protective material $\left[\mathrm{kg}/\mathrm{m}^3\right]$, taken as 957 kg/m^3;
c_p specific heat capacity of the protective material, assumed to be temperature-independent and equal to 1850 [J/(kg K)];
λ_p thermal conductivity of the protective material, equal to 0.45 [W/(m K)].

Prestress loss was estimated using a simplified linear relationship between temperature rise and reduction in the initial prestressing, based on the correlation between thermal elongation of the prestressing steel and the corresponding decrease in tendon axial force. The ultimate bending moment of the RC cross-section at each time step was then computed using the residual external prestressing force.

Because complete loss of prestressing occurred at time t_1, prior to the attainment of the 400 °C isotherm in the most exposed mild reinforcement of RC cross-section, at time t_2, the response in the interval $t_1 < t < t_2$ corresponds to that of the unstrengthened beam. For times greater than t_2, the ultimate bending capacity of the original beam further decreases due to the reduction in the yielding strength f_{yd} of the steel reinforcement, as prescribed by Eurocode 3 [33]. In the examined configuration, each deck beam is strengthened using two external tendons, each composed of four strands with a nominal diameter of 15 mm, with an initial prestressing value set to 1100 Mpa.

The degradation of mild reinforcement steel was evaluated through the coefficient k_θ provided by Eurocode 2, which affects the reduction in strength according to the following relation:

$$f_{\theta y} = k_\theta f_{yk} \tag{2}$$

where f_{yk} is the characteristic conventional yield strength (450 Mpa in the present case), and θ is the temperature at which the reduction is evaluated, based on the curve provided in Eurocode 2 for prestressing steel. The variation in k_θ with temperature is given by the following equation:

$$k_\theta = 1 - 0.45\frac{\theta - 400}{150} \tag{3}$$

Hence, the ultimate bending moment is computed, for each time and each temperature, according to the degraded value of steel yielding, using the above equations and taking into account axial force due to prestressing in the related *N*-*M* domain of cross-section.

3.2. Temperature and Structural Analysis for the Bridge with 10 m Span Length

Figure 7 shows the isotherms in the cross-section of the bridge beam with a 10 m span for the standard curve at 30 (Figure 7a) and 60 min (Figure 7b), and for the hydrocarbon curve, at 30 (Figure 7c) and 60 min (Figure 7d).

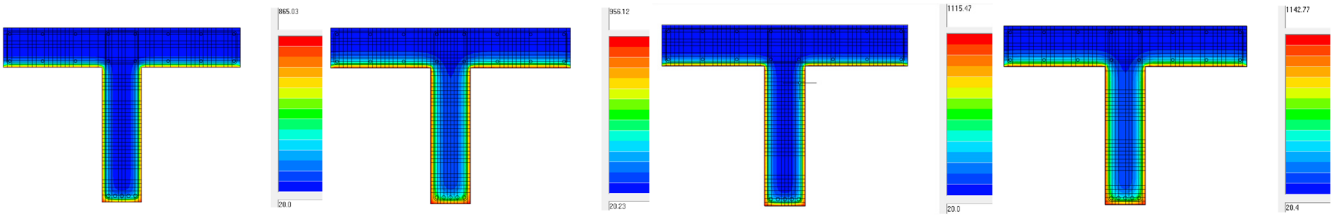

(**a**) (**b**) (**c**) (**d**)

Figure 7. Isothermal curves for the bridge beam (°C). (**a**) Standard curve at 30 min; (**b**) standard curve at 60 min; (**c**) hydrocarbon curve at 30 min; (**d**) hydrocarbon curve at 60 min.

Figure 8 presents the time-dependent evolution of the useful ultimate bending moment $M_{u,L}$ of the externally prestressed RC bridge exposed to both the standard and hydrocarbon fire curves, assuming a protective sheath thickness of 5 mm for each tendon. Both characteristic and frequent combinations of dead and traffic loads were considered, in accordance with the moving load models specified in Eurocode 1 [34]. Traffic loads were transversely distributed to the outermost beam, identified as the most heavily loaded, using the Courbon method.

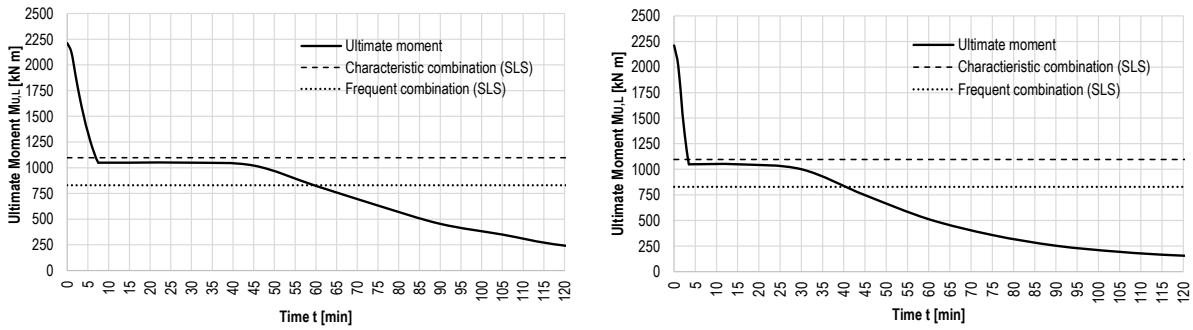

(**a**) (**b**)

Figure 8. Results of fire analysis on the bridge (10 m span). Ultimate moment and service loads with protective PE sheath 5 mm thick. (**a**) Standard curve; (**b**) hydrocarbon curve.

Due to prestressing degradation during fire, the ultimate bending moment decreases from the initial value of 2200 kNm (with prestressing) to the value that corresponds to the characteristic load combination (1100 kNm) approximately 7 min after fire ignition when the standard fire curve is applied. In contrast, the hydrocarbon fire reaches the same moment in less than 5 min.

Subsequently, the response of the RC section without external prestressing, corresponding to the horizontal plateau of the curves in Figure 8, reflects the residual performance of the RC bridge, which may be acceptable for lower traffic loads or when traffic has been stopped. The temperatures reported in Figure 7 are measured, for the RC section, at the bottom web reinforcement, as these are the most exposed and most relevant with respect to the ultimate bending moment of the simply supported beam. The plateau of the ultimate moment below the characteristic load combination represents the original RC ultimate moment prior to degradation of the mild reinforcement due to fire (1040 kNm). Consequently, under the standard fire scenario, failure corresponding to the value of ultimate moment equal to that of the frequent load combination occurs after approximately 60 min.

Under hydrocarbon fire exposure, the corresponding failure time is reduced to around 40 min. This indicates that, for the frequent combination of moving loads, the bridge retains sufficient load-bearing capacity for a duration adequate to ensure safety following the accident and fire ignition. In contrast, the characteristic load combination is not maintained for a time interval compatible with the arrival of rescue teams and the implementation of traffic interruption measures. All evaluations assume unitary strength safety factors.

Because the structural response under the maximum moving load combination is governed by the fast degradation of the external prestressing tendon properties and the associated abrupt loss of prestressing force, the analyses were extended by considering an increased thickness of the protective sheath. Figure 9 reports the evolution of the ultimate bending moment under the standard fire exposure (Figure 9a) and the hydrocarbon fire scenario (Figure 9b), assuming a polyethylene (PE) sheath thickness of 15 mm.

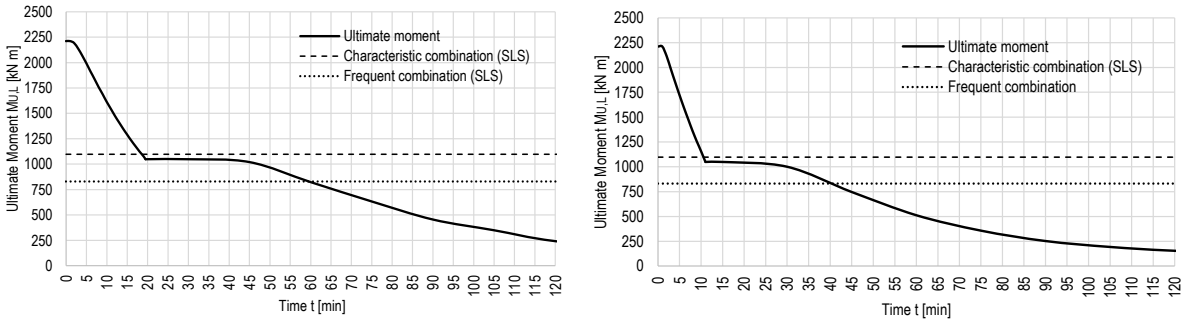

(**a**) (**b**)

Figure 9. Results of fire analysis on the bridge (10 m span). Ultimate moment and service loads with protective PE sheath 15 mm thick. (**a**) Standard curve; (**b**) hydrocarbon curve.

Under this configuration, the response of the externally prestressed system becomes significantly more gradual, resulting in a delayed attainment of the critical condition associated with the characteristic load combination. Specifically, failure occurs after approximately 18 min under the standard fire curve and about 10 min under the hydrocarbon fire curve. These times are nearly twice those obtained with the thinner protective sheath and provide a minimum reaction window before structural damage may lead to severe consequences under high traffic load conditions.

It is noted that the increase in sheath thickness primarily influences the load-bearing capacity associated with the characteristic load combination, while it does not affect the behavior of the RC cross-section and the limit corresponding to the frequent load combination. Accordingly, the fire-induced response of the unprestressed RC section remains unchanged.

These results suggest that the fire performance of externally strengthened structures can be substantially improved through the use of more effective protective sheaths for external tendons. Such protection should not be designed solely to facilitate tendon movement or to ensure durability against environmental exposure, as is common in engineering practice, but should be deliberately enhanced to improve structural performance under accidental fire scenarios.

Table 3 summarizes the times for the different cases. Time t_1 corresponds to the total loss of prestressing and the attainment of the ultimate moment of the original RC beam (plateau), t_2 indicates the onset of degradation of mild reinforcements in the RC beam, while t_{char} is the time at which the ultimate moment of the degraded beam reaches the characteristic load combination level, and t_{freq} corresponds to the time at which the ultimate moment reaches the level of the frequent load combination.

Table 3. Time results for the bridge span of 10 m.

Fire Curve	Protective PE Sheath [mm]	t_1 [min]	t_2 [min]	t_{char} [min]	t_{freq} [min]
Standard	5	8	40	7	60
	15	18	40	16	60
Hydrocarbon	5	4	25	3	40
	15	12	25	10	40

The analysis was repeated using the temperatures recorded by the CFD model in the fire Scenario FS1 at the beam web, which were found to be the lowest ones, with a sustained temperature of 850 °C. The temperatures within the cross-section were derived, and the temperature–time curves of the prestressing tendon with a 15 mm protective sheath and of the original reinforced concrete (RC) section were determined. Figure 10a compares the three temperature curves: the nominal hydrocarbon fire curve, the gas temperature at the beam web obtained from the CFD model (FS1), and the temperature curve reached by the mild steel reinforcement within the RC section.

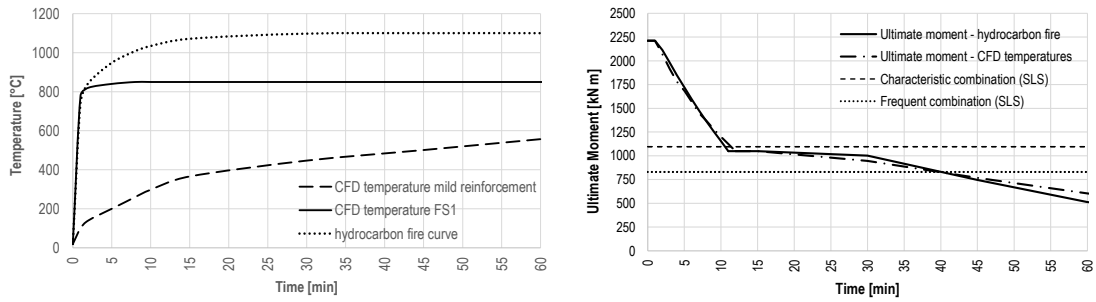

(**a**) (**b**)

Figure 10. Comparison of results of fire analysis on the bridge (10 m span) with CFD temperatures of fire load FS1 and hydrocarbon fire curve. (**a**) Temperature-time curves; (**b**) ultimate moment.

Figure 10b shows the ultimate bending moment degradation of the beam, comparing the results obtained using the nominal hydrocarbon fire curve with those obtained using the temperature histories from the CFD model reported in Figure 10a. It can be observed that the rapid initial increase in temperature, which is characteristic of hydrocarbon fire exposure, plays a decisive role in the degradation process. As a result, the outcomes obtained using the nominal fire curve are essentially coincident with those derived from the CFD-based temperature histories during the first 60 min of exposure. This occurs even if the sustained temperature in the CFD simulation is lower than that of the code curve, because during the stage of prestressing relaxation, the concrete still has time to heat up, and the internal temperatures of the bottom reinforcement do not differ significantly from those observed in thermal analyses based on literature fire curves. Consequently, the use of nominal fire curves is validated for the case study of highway overpasses subjected to tanker accident scenarios, even when the final temperatures are lower than those of the hydrocarbon fire curve, since the critical degradation occurs within the first 60 min. The ultimate bending moment corresponding to the frequent load combination is reached at 40 min, confirming the results previously presented in Figure 9.

This comparison thus supports the use of simplified approaches in hydrocarbon fire risk assessments for highway overpasses, where the standard nominal fire curve can be considered a lower-bound scenario, and the hydrocarbon fire curve represents an upper-bound, severe scenario. The actual temperature histories obtained from CFD analysis fall

between these two curves, but are characterized by a rapid initial temperature rise, which is critical for assessing structural behavior during the early stages of the fire.

3.3. Temperature and Structural Analysis for the Bridge with 15 m Span Length

Similar analyses were also conducted on the bridge configuration composed of five beams with a span length of 15 m (Figure 1c,d). As in the previous cases, four external prestressing tendons with a nominal diameter of 15 mm were adopted, each tensioned to an initial stress level of 1100 MPa. The parametric study again considered variations in both the applied fire exposure curve and the thickness of the protective sheath surrounding the tendons. Overpass clearance height was fixed to 8 m.

Figure 11 presents the temperature analysis performed on the T-shaped cross-section of the main beam. The load application followed the same procedure as in the previous case, with actions applied to the outermost beam of the deck, identified as the most critical in terms of loading. The ultimate bending moment was assessed throughout the progressive degradation of external prestressing induced by fire exposure. Once the prestressing system became ineffective, the structural response of the RC beam without external prestressing was subsequently evaluated.

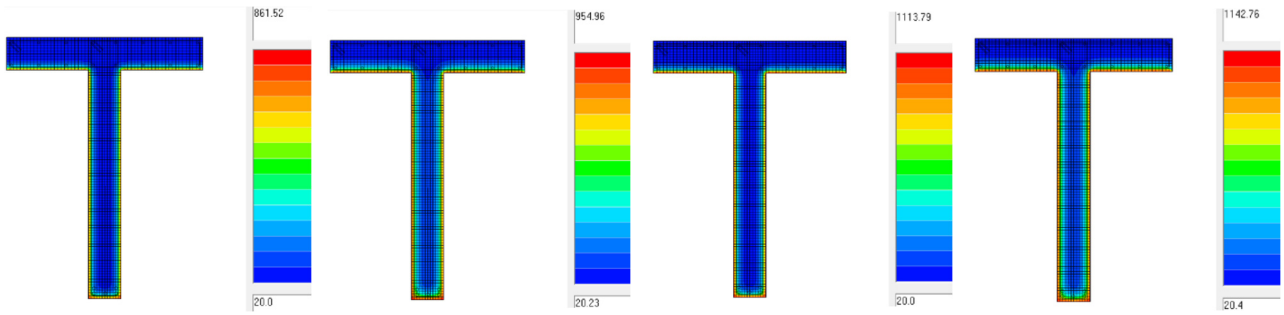

(**a**) (**b**) (**c**) (**d**)

Figure 11. Isothermal curves (°C) for the bridge beam of 15 m span. (**a**) Standard curve at 30 min; (**b**) standard curve at 60 min; (**c**) hydrocarbon curve at 30 min; (**d**) hydrocarbon curve at 60 min.

Figure 12 shows the progression of the ultimate moment, and the levels of the load combinations reached for standard fire and hydrocarbon fire with a 5 mm thin cable sheath protection.

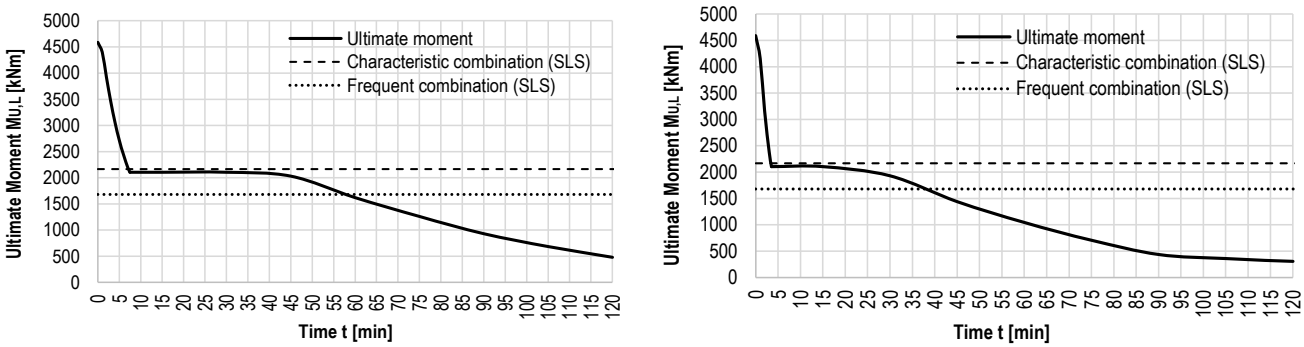

(**a**) (**b**)

Figure 12. Results of fire analysis on the bridge (15 m span). Ultimate moment and service loads with protective PE sheath 5 mm thick. (**a**) Standard curve; (**b**) hydrocarbon curve.

In this case, the ultimate moment of the beam strengthened with external prestressing is 4400 kNm, which subsequently decreases due to prestressing degradation caused by fire, reaching the level corresponding to the characteristic load combination at 2170 kNm.

Similarly, the plateau of the ultimate moment of the original RC beam, without prestressing, is below that required by the characteristic combination, while the moment corresponding to the frequent load combination is 1680 kNm. This value is reached by the effective ultimate moment after reinforcement degradation of the original RC section, occurring at 55 min for the standard fire curve and 37 min for the hydrocarbon one.

Figure 13 presents the results with a 15 mm protective sheath, showing the improved performance of the prestressed beam, which degrades more slowly, reaching the characteristic combination moment level at 18 min for the standard fire curve (Figure 13a), compared to 7 min in Figure 12a with the 5 mm sheath. For the hydrocarbon fire curve, the same level is reached at 10 min (Figure 13b), instead of 3 min for the 5 mm sheath.

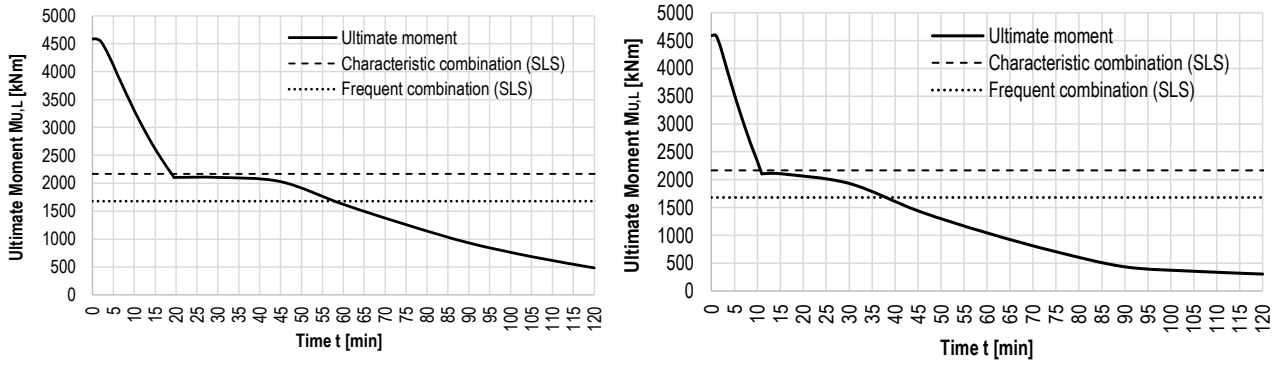

(**a**) (**b**)

Figure 13. Results of fire analysis on the bridge (15 m span). Ultimate moment and service loads with protective PE sheath 15 mm thick. (**a**) Standard curve; (**b**) hydrocarbon curve.

Table 4 summarizes the times achieved for the different cases analyzed for the bridge of 15 m span. The decisive role of the protective sheath thickness is thus confirmed. The differences in the times identified with respect to the 10 m bridge case mainly arise from the thermal analysis of the cross-section, which features a different geometry exposed to fire and a different configuration of the bottom mild reinforcement.

Table 4. Time results for the 15 m bridge span.

Fire Curve	Protective PE Sheath [mm]	t_1 [min]	t_2 [min]	t_{char} [min]	t_{freq} [min]
Standard	5	8	40	7	60
	15	19	40	18	60
Hydrocarbon	5	4	22	3	37
	15	12	22	10	37

The time required to reach different performance levels in terms of load-bearing capacity and ultimate bending moment is directly related to the time available for traffic closure and emergency response. Accordingly, a longer initial delay before the prestress loss is essential to ensure sufficient reaction time and to prevent heavy vehicle loads on the bridge, potentially occurring within the first minutes after fire ignition, from inducing early-stage damage. This enables timely traffic restrictions or closure, allowing emergency services to operate effectively. Consequently, increasing the thickness of the protective sheath represents both a feasible maintenance strategy for existing strengthened bridges and a design option for new retrofit systems. Hence, extending the time t_1 from 4 to 12 min is important to achieving improved structural performance and reduced fire-related risk.

3.4. Influence of Degradation in Multi-Risk Assessment

To account for the possible simultaneous presence of pre-existing degradation of the original RC section or aging of the external prestressing retrofit, related to a fire event in a multi-hazard context, several scenarios were analyzed for the 10 m-span bridge:

Scenario A → Fire + RC section degradation.
Scenario B → Fire + prestressing tendon corrosion.
Scenario C → Fire + RC section degradation + prestressing tendon corrosion.
Scenario D → Fire + advanced degradation of the RC section.

In Scenario A, the effects of RC section degradation and its impact on the performance of the beam under fire exposure are considered. It is assumed that, over time since the bridge's construction, the beam section has experienced degradation affecting both the concrete and the reinforcement. Specifically, the reinforcement bars are assumed to have lost 10–20% of their cross-sectional area due to corrosion, while the concrete strength is reduced to 85% due to carbonation and cracking. Furthermore, at the time of the strengthening intervention, the original reinforcement was not restored and thus remained degraded.

This degradation naturally reduces the performance of the original RC beam, resulting in a lower ultimate moment compared to an intact cross-section. By applying the same procedures used in the previous cases for both thermal and mechanical analyses, the time-dependent reduction in the ultimate moment is obtained.

Figure 14 shows the results for Scenario A, indicating a reduction in the ultimate moment in the latter part of the curve, representing the behavior of the RC section. The initial portion of the curve remains unchanged in shape, but it is shifted downward due to the lower ultimate moment of the degraded RC beam. Consequently, failure under the characteristic load combination occurs at times very similar to those of the beam without degradation. The same applies to time t_1, which represents the loss of prestressing effect, occurring at the same instant regardless of the degradation state.

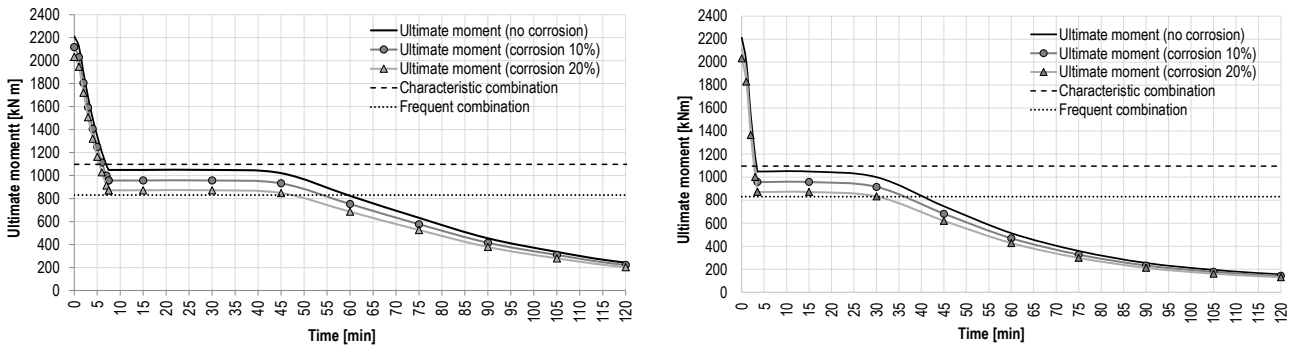

(**a**) (**b**)

Figure 14. Results of fire analysis on the bridge of 10 m span for multi-risk Scenario A. (**a**) Standard curve; (**b**) hydrocarbon curve.

Conversely, the attainment of failure for the frequent load combination shows noticeable variations depending on the level of degradation. For the standard fire curve, for instance, it is reached after approximately 47 min with 20% reinforcement corrosion, compared to 60 min without degradation. For the hydrocarbon curve, the time decreases from 40 to 30 min under the effect of 20% corrosion.

In the multi-risk Scenario B, it is assumed that, over time, after the strengthening intervention, the strands of the prestressing tendon begin to corrode. This is because, being externally positioned and despite being protected by a plastic sheath, they are still exposed to atmospheric agents. The possible corrosion of the external prestressing anchorages is

also considered. As a result of corrosion on the strands and anchorages, a 20% prestressing loss is assumed. In other words, the tendon undergoes a relaxation corresponding to 20% of the initial prestress: the original axial force of 1200 kN for the single beam section is thus reduced to 960 kN. Once this assumption is established, the same procedure used previously is followed. Figure 15 presents the results obtained.

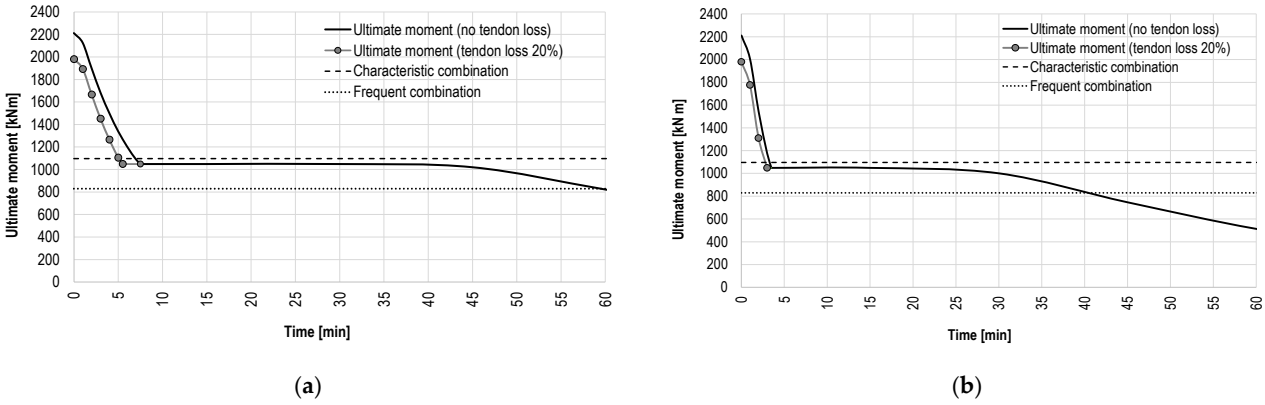

(**a**) (**b**)

Figure 15. Results of fire analysis on the bridge of 10 m span for multi-risk Scenario B. (**a**) Standard curve; (**b**) hydrocarbon curve.

This Scenario affects only the initial portion of the degradation curve. It is observed that, for the standard and external fire curves, the tendon relaxation leads to the attainment of failure for the characteristic load combination approximately 2 min earlier compared to 7 min in the condition without relaxation. In contrast, for the hydrocarbon fire curve, only a minimal difference is observed, as this fire scenario is already particularly severe even without any prestress loss in the tendon.

The multi-risk Scenario C is a combination of the previous A and B. It is thus assumed that the fire event occurs simultaneously with both the degradation of the RC section and the loss of prestressing in the external tendon. This scenario is therefore more severe from a multi-risk perspective, as it involves the consideration of three risk factors.

Although the likelihood of such a Scenario occurring is certainly lower, it is still important to evaluate it, since the resulting damage and consequences can be highly critical, making the associated risk level significant. It should also be noted that, in the context of existing bridges, such degradation phenomena are often frequent, particularly for older structures; therefore, this study provides a valuable tool for assessing the vulnerability of these bridges. Figure 16 presents the results obtained for the combined scenario C.

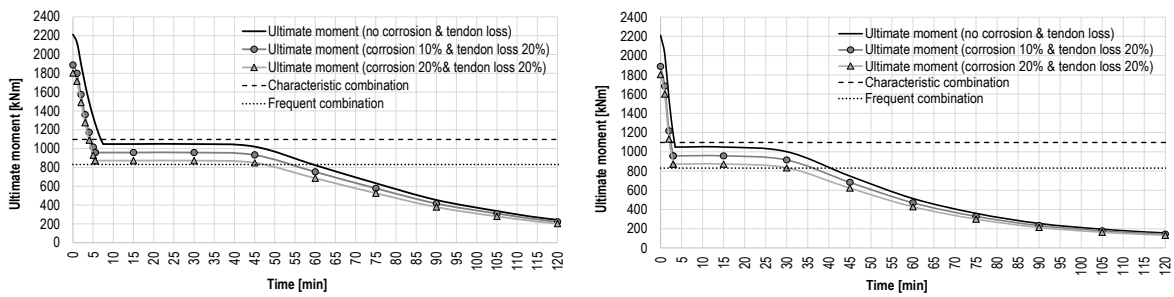

(**a**) (**b**)

Figure 16. Results of fire analysis on the bridge of 10 m span for multi-risk Scenario C. (**a**) Standard curve; (**b**) hydrocarbon curve.

In Scenario C, performance decay affects both the early and later portions of the degradation curve, combining the effects of the previous scenarios. Corrosion in both the

beam and tendon has little impact on overall structural response. The key factor for fire performance is whether the strengthening intervention included restoration of concrete and reinforcement. Fire risk is governed primarily by degradation of the original RC beam, as prestressing is lost relatively early. Restoring both concrete and steel improves fire performance, whereas leaving pre-existing degradation unaddressed—relying solely on prestressing—creates a critical multi-risk scenario.

The impact of Scenario C is particularly pronounced when beam degradation occurs before tendon prestress is fully lost. This can happen if the beam is already heavily degraded or if prestress loss is delayed, for instance by a thicker protective tendon sheath. A realistic example occurs when the bottom concrete cover is missing, leaving the reinforcement exposed and causing premature degradation of the RC cross-section.

Scenario D is then designed to illustrate this behavior. It assumes an advanced state of beam degradation with concrete cover detachment, exposing corroded reinforcement with an assumed 20% reduction in bar cross-section. The concrete itself is significantly degraded, with strength reduced to 80% of its original value f_c. Additionally, the prestressing tendon is assumed to be protected by a thicker sheath of 15 mm.

This scenario may also result from concrete cover detachment due to spalling during the initial heating phase. In such cases, the effect is equivalent if the cover is removed explosively, depending on the type of aggregates and concrete exposed to fire. Fire-induced spalling directly exposes the mild reinforcement to the fire, accelerating the degradation of the RC beam due to the loss of protective skin concrete. To account for this effect, the isotherms of the new section without concrete cover are newly evaluated, resulting in much faster heat transfer to the exposed reinforcement bars and consequently a more rapid degradation of the section's ultimate moment capacity. The steel degradation is assessed as in previous cases, by reducing the yielding stress f_{yk} of steel according to the temperature reached.

Results of the analysis are presented in Figure 17. It is observed that, in this case, the original beam begins to degrade much earlier. Here, the multi-risk scenario of fire plus degradation becomes significant. The section degradation starts even before the prestressing loss, so the two curves intersect and the horizontal segment of RC bending moment plateau disappears. Time t_2, marking the onset of RC section degradation, now precedes time t_1, which indicates when the effect of the external prestressing is lost. Consequently, the frequent load combination—and, of course, the characteristic one—is reached along the initial portion of the curve, before the prestress effect in the external tendon is lost.

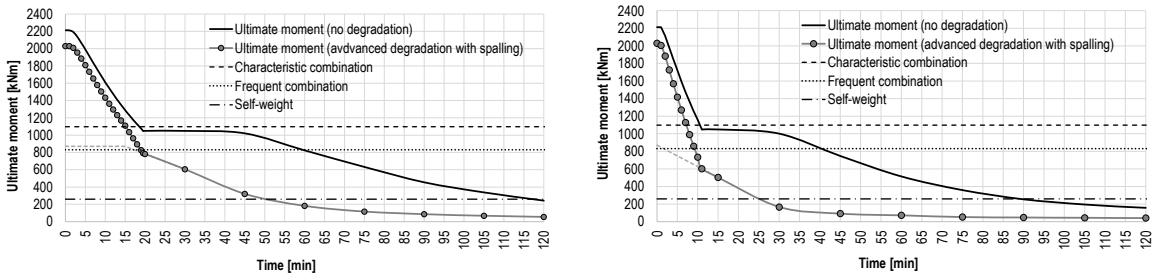

(**a**) (**b**)

Figure 17. Results of fire analysis on the bridge of 10 m span for multi-risk Scenario D. (**a**) Standard curve; (**b**) hydrocarbon curve. The grey dash line is not effective since it is related to the unprestressed element before prestressing relaxation happens.

With such a pronounced degradation curve, observations can also be made regarding the attainment of the load combination under dead load only, i.e., the condition in which the bridge would fail due solely to self-weight and imposed loads if the fire persists for

a certain period. Specifically, for the standard fire curve, this condition is reached after approximately 50 min (Figure 17a), while for the hydrocarbon curve it occurs after just 25 min of fire exposure (Figure 17b). This time interval becomes critical, as it may not be possible to secure the area with emergency response teams before collapse.

For the intact beam, by contrast, reaching this combination was not critical, occurring after 90 min for the hydrocarbon curve and 120 min for the standard curve. For the external fire curve, although premature section degradation and faster performance decay are observed, no risk of collapse arises even after extended exposure times.

This confirms that, when the beam remained degraded without restoration at the time of external strengthening, the combined effect of the two risks could lead to a critical condition, potentially resulting in collapse. It is further highlighted that the prestressing retrofit does not delay collapse, which depends solely on the degradation of the original beam. The strengthening intervention serves only to postpone the attainment of the ultimate moment corresponding to the characteristic and frequent load combinations, i.e., with traffic present during fire exposure.

The results show that the key factor governing this behavior is the earlier onset of degradation of the RC cross-section, which occurs after approximately 15 min for the standard fire curve and coincides with the start of the fire for the hydrocarbon curve. No differences are observed in the times t_1 associated with the loss of tendon prestressing, since corrosion of the anchorages is not considered.

In this multi-risk Scenario D, the attainment of the characteristic load combination is anticipated by a few minutes in all fire conditions. A more significant difference is observed for the frequent load combination, which is now intersected by the initial portion of the degradation curve and therefore reached much earlier than in the non-degraded bridge. Finally, as previously noted, under such an advanced degradation state, the potential collapse of the bridge due to the attainment of the dead load combination becomes a concern, both for the standard fire curve and, more critically, for the hydrocarbon fire curve.

This scenario severely limits the available time for the arrival of the emergency response team, as the rapid degradation of prestressing leads to an immediate reduction in load-bearing capacity, causing the bridge to reach a critical risk of collapse earlier than in the case of an intact bridge (25 min).

Table 5 summarizes the results in terms of the time required to reach the various significant states for the different scenarios considered. For the last scenario, the time t_{dead} of attainment of the ultimate moment, corresponding to that of only dead load applied to the bridge, is considered.

Table 5. Time results in a bridge of 10 m span in multi-risk scenarios.

Multi-Risk Scenario	Fire Curve	t_1 [min]	t_{char} [min]	t_{freq} [min]	t_{dead} [min]
Undegraded bridge	Standard	8	7	60	-
	Hydrocarbon	19	18	60	-
Scenario 1 (mild steel corrosion)	Standard	8	5	47	-
	Hydrocarbon	4	3	30	-
Scenario 2 (tendon loss)	Standard	6	5	60	-
	Hydrocarbon	3	3	40	-
Scenario 3 (steel corrosion + tendon loss)	Standard	5	4	47	-
	Hydrocarbon	3	2	30	-
Scenario 4 (advanced degradation + spalling)	Standard	19	15	18	50
	Hydrocarbon	11	7	9	25

4. Conclusions

This study investigated the fire performance of existing RC bridge decks strengthened by external prestressing systems, with particular attention to the influence of load level and prestressing effectiveness on structural safety during fire events. A comprehensive assessment framework was developed and applied to representative bridge configurations, with the aim of evaluating the degradation of structural capacity under fire exposure and identifying critical conditions that may lead to failure even at load levels lower than those generally considered at the Ultimate Limit State.

The thermal input adopted for the analyses was validated through a dedicated computational fluid dynamics (CFD) study, which allowed the evaluation of temperature development in typical highway overpass bridge decks characterized by RC beam–girder grillage systems. The CFD analyses considered variations in clearance height and span length and confirmed that, in the case of hydrocarbon tanker accidents with fuel spilled on the roadway, the use of conventional fire curves available in the literature provides an adequate representation of both the temperature levels reached and the rate of temperature increase within the structural elements. This validation supports the applicability of simplified fire curves for speedy and preliminary assessments in realistic accident scenarios for the risk assessment of large stocks of existing bridges within the roadway network.

The structural response under fire was evaluated through an analytical fire safety procedure for several realistic bridge case studies. Thermal and mechanical analyses were performed by varying deck cross-sections, span lengths, ordinary reinforcement layouts, and the presence of external prestressing retrofit, allowing for a parametric investigation of the degradation of mechanical properties over time. The reduction in the ultimate bending capacity of bridge decks was assessed through numerical analyses by evaluating the reduction in ultimate moment for the most stressed girder sections.

Results highlight the critical role of external prestressing systems in fire scenarios. While external prestressing is effective under ordinary service conditions, the rapid degradation of tendon capacity and prestressing force during fire exposure may lead to critical situations even for load combinations associated with serviceability. Frequent load combinations were generally found to remain below the residual bending capacity of the RC members, ensuring acceptable performance and providing a sufficient time window for emergency response and traffic management. Nevertheless, the protection of external tendons emerges as a key factor in ensuring structural robustness, as the loss of prestressing effectiveness strongly influences the residual capacity during and after fire events.

Finally, within a multi-hazard assessment framework, the combined effects of fire exposure and pre-existing structural deterioration were investigated. Aging-related degradation mechanisms, such as corrosion of the original reinforcement and long-term reductions in external prestressing force, were shown to significantly increase the vulnerability of externally prestressed bridges under fire. The rapid loss of prestressing effectiveness during the initial minutes of fire exposure amplifies the adverse effects of prior deterioration, worsening the condition of the original RC structure and increasing the risk of failure. In the most severe multi-risk scenarios, phenomena such as corrosion-induced spalling or early explosive spalling of the concrete cover may lead to a rapid temperature increase in the effective reinforcement and, combined with the loss of prestressing contribution, result in premature collapse under dead loads. These findings emphasize the importance of integrating fire safety considerations with aging and deterioration effects in performance-based assessment and design strategies for existing bridge infrastructure.

Author Contributions: Conceptualization, methodology, validation, formal analysis, investigation, data curation, writing—original draft preparation, writing—review and editing, M.F.G. Methodology,

validation, analysis, data curation, writing—review and editing, Z.-C.G. Methodology, validation, investigation, data curation, writing—review and editing, P.C. All authors have read and agreed to the published version of the manuscript.

Funding: Acknowledgements are due to the Italian Ministry of University and Research for the research grant in the PRIN PNRR 2022 line, under the project SaFeBIMAs: Estimation of the combined Seismic-Fire risk and optimization of interventions for Buildings and Infrastructures in the context of Metropolitan Areas.

Data Availability Statement: Data are available from the author on reasonable request.

Acknowledgments: The authors wish to acknowledge Mario Stabile and Antonio Cutrona for supporting the authors in the execution of some analyses. The authors are also grateful to Thunderhead Engineering Consultants Inc., USA, for providing the free education license for PyroSim—a graphic user interface for FDS.

Conflicts of Interest: The authors declare no conflicts of interest.

References

1. Hu, J.; Carcel, R.; Usmani, A. Bridge fires in the 21st century: A literature review. *Fire Saf. J.* **2021**, *126*, 103487. [CrossRef]
2. Garlock, M.; Paya-Zaforteza, I.; Kodur, V.; Li, G. Fire hazard in bridges: Review, assessment and repair strategies. In *Engineering Structures*; Elsevier: Amsterdam, The Netherlands, 2012; Volume 35, pp. 89–98.
3. Kodur, V.K.R.; Gu, L.; Garlock, M.E.M. Review and assessment of fire hazard in bridges. *Transp. Res. Rec. J. Transp. Res. Board.* **2010**, *2172*, 23–29. [CrossRef]
4. Lee, G.C.; Mohan, S.B.; Huang, C.; Fard, B.N. *Technical Report MCEER-13-008: A Study of US Bridge Failures (1980–2012)*; MCEER, University at Buffalo (SUNY): Buffalo, NY, USA, 2013.
5. Zhang, G.; Zhao, X.; Lu, Z.; Song, C.; Li, X.; Tang, C. Review and discussion on fire behaviour of bridge girders. *J. Traffic Transp. Eng. (Engl. Ed.)* **2022**, *9*, 422–446.
6. Kodur, V.K.R.; Naser, M.Z. Importance factor for design of bridges against fire. *Eng. Struct.* **2013**, *54*, 207–220. [CrossRef]
7. Jeyashree, T.M.; Kannan Rajkumar, P.R.; Satyanarayanan, K.S. Developments and research on fire response behaviour of prestressed concrete members—A review. *J. Build. Eng.* **2022**, *57*, 104797. [CrossRef]
8. Liu, Z.; Xie, H.; Han, B.; Li, P.; Jiang, Z.; Yu, J. Experimental study on residual bearing capacity of full-size fire-damaged prestressed concrete girders. *Structures* **2022**, *45*, 1788–1802. [CrossRef]
9. Recupero, A.; Spinella, N.; Colajanni, P.; Scilipoti, C.D. Increasing the Capacity of Existing Bridges by Using Unbonded Prestressing Technology: A Case Study. *Adv. Civ. Eng.* **2014**, *2014*, 840902. [CrossRef]
10. Granata, M.F.; Recupero, A.; Culotta, G.; Arici, M. Influence of axial force and corrosion on failure of prestressed concrete structures considering M-V interaction. *Eng. Struct.* **2021**, *242*, 112552. [CrossRef]
11. Granata, M.F.; La Mendola, L.; Messina, D.; Recupero, A. Assessment and strengthening of reinforced concrete bridges with half-joint deterioration. *Struct. Concr.* **2023**, *24*, 269–287. [CrossRef]
12. Jeanneret, C.; Nicoletta, B.; Robertson, L.; Gales, J.; Kotsovinos, P. Guidance for the post-fire structural assessment of prestressing steel. *Eng. Struct.* **2021**, *235*, 112023. [CrossRef]
13. De Silva, D.; Gallo, M.; De Falco, L.; Nigro, E. Fire risk assessment of bridges: From state of the art to structural vulnerability mitigation. *J. Civ. Struct. Health Monit.* **2023**, *13*, 1613–1632. [CrossRef]
14. Atienza, J.M.; Elices, M. Behavior of prestressing steels after a simulated fire: Fire-induced damages. *Constr. Build. Mater.* **2009**, *23*, 2932–2940. [CrossRef]
15. Kotsovinos, P.; Judge, R.; Walker, G.; Woodburn, P. Fire Performance of Structural Cables: Current Understanding, Knowledge Gaps, and Proposed Research Agenda. *J. Struct. Eng. ASCE* **2020**, *146*, 03120002. [CrossRef]
16. Bamonte, P.; Kalaba, N.; Felicetti, R. Computational study on prestressed concrete members exposed to natural fires. *Fire Saf. J.* **2018**, *97*, 54–65. [CrossRef]
17. Eamon, C.D.; Jensen, E. Reliability analysis of prestressed concrete beams exposed to fire. *Eng. Struct.* **2012**, *43*, 69–77. [CrossRef]
18. Wu, X.; Huang, T.; Au, F.T.K.; Li, J. Posttensioned Concrete Bridge Beams Exposed to Hydrocarbon Fire. *J. Struct. Eng. ASCE* **2020**, *146*, 04020210. [CrossRef]
19. Ellobody, E.; Bailey, C.G. Modelling of unbonded post-tensioned concrete slabs under fire conditions. *Fire Saf. J.* **2009**, *44*, 159–167. [CrossRef]
20. Gales, J.; Bisby, L.A.; MacDougall, C.; MacLean, K. Transient high-temperature stress relaxation of prestressing tendons in unbonded construction. *Fire Saf. J.* **2009**, *44*, 570–579. [CrossRef]

21. Gales, J.; Bisby, L.A.; Gillie, M. Unbonded post tensioned concrete in fire: A review of data from furnace tests and real fires. *Fire Saf. J.* **2011**, *46*, 151–163. [CrossRef]
22. Colajanni, P.; Recupero, A.; Spinella, N. Design procedure for prestressed concrete beams. *Comput. Concr.* **2014**, *13*, 235–253. [CrossRef]
23. Granata, M.F.; Colajanni, P.; Arfeli, L.; La Mendola, L. Experimental campaign for sustainable repair of RC beamscwith unbonded prestressing. American Concrete Institute Special Publication. In Proceedings of the 3rd International Workshop on "Durability and Sustainability of Concrete Structures" (DSCS 2025), Naples, Italy, 16–18 September 2025.
24. *Eurocode 1: Actions on Structures, Part 1–2: General Actions—Actions on Structures Exposed to Fire*; CEN (European Committee for Standardization): Brussels, Belgium, 2002.
25. Peris-Sayol, G.; Paya-Zaforteza, I.; Alos-Moya, J.; Hospitaler, A. Analysis of the influence of geometric, modeling and environmental parameters on the fire response of steel bridges subjected to realistic fire scenarios. *Comput. Struct.* **2015**, *158*, 333–345. [CrossRef]
26. Gernay, T. Performance-based design for structures in fire: Advances, challenges, and perspectives. *Fire Saf. J.* **2024**, *142*, 104036. [CrossRef]
27. McGrattan, K.; Hostikka, S.; Floyd, J.; McDermott, R.; Vanella, M.; Mueller, E. *Fire Dynamics Simulator—User's Guide*, 6th ed.; NIST Special Publication 1019; National Institute of Standards and Technology: Gaithersburg, MD, USA, 2024.
28. McGrattan, K.; Hostikka, S.; Floyd, J.; McDermott, R.; Vanella, M.; Mueller, E. *Fire Dynamics Simulator, Technical Reference Guide, Volume 1: Mathematical Model*, 6th ed.; NIST Special Publication 1018-1; National Institute of Standards and Technology: Gaithersburg, MD, USA, 2024.
29. McGrattan, K.; Hostikka, S.; Floyd, J.; McDermott, R.; Vanella, M.; Mueller, E. *Fire Dynamics Simulator, Technical Reference Guide, Volume 2: Verification*, 6th ed.; NIST Special Publication 1018-2; National Institute of Standards and Technology: Gaithersburg, MD, USA, 2024.
30. McGrattan, K.; Hostikka, S.; Floyd, J.; McDermott, R.; Vanella, M.; Mueller, E. *Fire Dynamics Simulator, Technical Reference Guide, Volume 3: Validation*, 6th ed.; NIST Special Publication 1018-3; National Institute of Standards and Technology: Gaithersburg, MD, USA, 2024.
31. Babrauskas, V. Volume I, 25 Heat Release Rates. In *SFPE Handbook of Fire Protection Engineering*, 5th ed.; Springer: Berlin/Heidelberg, Germany, 2023; pp. 799–904.
32. Gottuk, D.T.; White, D.A. Volume III, Liquid Fuel Fires. In *SFPE Handbook of Fire Protection Engineering*, 5th ed.; Springer: Berlin/Heidelberg, Germany, 2023; pp. 2552–2590.
33. *Eurocode 3: Design of Steel Structures, Part 1–2: General Rules—Structural Fire Design*; CEN (European Committee for Standardization): Brussels, Belgium, 2005.
34. *EN 1991-2*; Traffic Loads on Bridges, Part 2. Eurocode 1. CEN (European Committee for Standardization): Brussels, Belgium, 2005.

Disclaimer/Publisher's Note: The statements, opinions and data contained in all publications are solely those of the individual author(s) and contributor(s) and not of MDPI and/or the editor(s). MDPI and/or the editor(s) disclaim responsibility for any injury to people or property resulting from any ideas, methods, instructions or products referred to in the content.